Crystal Structure of the Cysteine-rich Domain of Mannose Receptor Complexed with a Sulfated Carbohydrate Ligand

By Yang Liu,* Arthur J. Chirino,*‡ Ziva Misulovin,§ Christine Leteux,‖ Ten Feizi,‖ Michel C. Nussenzweig,§ and Pamela J. Bjorkman*‡

*From the *Division of Biology 156-29 and the ‡Howard Hughes Medical Institute, California Institute of Technology, Pasadena, California 91125; the §Department of Molecular Immunology and the Howard Hughes Medical Institute, The Rockefeller University, New York, New York 10021-6399; and the ‖Glycosciences Laboratory, Imperial College School of Medicine, Northwick Park Hospital, Harrow HA1 3UJ, United Kingdom*

Abstract

The macrophage and epithelial cell mannose receptor (MR) binds carbohydrates on foreign and host molecules. Two portions of MR recognize carbohydrates: tandemly arranged C-type lectin domains facilitate carbohydrate-dependent macrophage uptake of infectious organisms, and the NH_2-terminal cysteine-rich domain (Cys-MR) binds to sulfated glycoproteins including pituitary hormones. To elucidate the mechanism of sulfated carbohydrate recognition, we determined crystal structures of Cys-MR alone and complexed with 4-sulfated-*N*-acetylgalactosamine at 1.7 and 2.2 Å resolution, respectively. Cys-MR folds into an approximately three-fold symmetric β-trefoil shape resembling fibroblast growth factor. The sulfate portions of 4-sulfated-*N*-acetylgalactosamine and an unidentified ligand found in the native crystals bind in a neutral pocket in the third lobe. We use the structures to rationalize the carbohydrate binding specificities of Cys-MR and compare the recognition properties of Cys-MR with other β-trefoil proteins.

Key words: β-trefoil protein • hydrogen bond network • multilectin receptor • pituitary hormones • sulfated GalNAc

Introduction

The innate immune response is critical for detection and elimination of infectious microorganisms. Carbohydrates on microbial cell walls are common targets for pattern recognition receptors on immune cells such as macrophages, which recognize a variety of antigens (1). The mannose receptor (MR),[1] expressed on some macrophages, epithelial, and endothial cells (2, 3), is the prototype member of a family of multilectin receptors that recognize carbohydrates on the cell walls of infectious organisms (4). Carbohydrate recognition by MR facilitates macrophage uptake of bacteria, yeast, and parasites, thereby contributing to innate immunity towards these pathogens. MR is also thought to play a role in the adaptive immune response by transporting antigens to MHC class II–containing compartments in immature dendritic cells for antigen processing and presentation to T cells (5), and by delivering mycobacterially derived glycolipids to endosomes for T cell presentation by the MHC class I–like molecule CD1b (6).

MR is a 180-kD type I transmembrane protein that contains three extracellular regions: an NH_2-terminal cysteine-rich domain (Cys-MR), a domain containing fibronectin type II repeats, and eight tandem C-type lectin carbohydrate-recognition domains (CRDs; 4). The extracellular domains are linked to a transmembrane region and a small cytoplasmic domain. These structural characteristics are shared among members of the MR family, which includes the phospholipase A2 receptor (7–9), the dendritic cell receptor DEC-205 (10), and an MR-like receptor expressed in epithelium (11). The CRDs of the extracellular region mediate calcium-dependent binding to sugars such as mannose, fucose, and *N*-acetylglucosamine that are commonly found on microorganisms, but rarely seen in sufficient density in terminal positions of mammalian oligosaccharides

Address correspondence to Pamela J. Bjorkman, Division of Biology 156-29, California Institute of Technology, Pasadena, CA 91125. Phone: 626-395-8350; Fax: 626-792-3683; E-mail: bjorkman@cco.caltech.edu

[1]*Abbreviations used in this paper:* 4-SO_4-GalNAc, 4-sulfated-*N*-acetylgalactosamine; aFGF, acidic FGF; bFGF, basic FGF; CRD, carbohydrate-recognition domain; Cys-MR, cysteine-rich domain of the MR; FGF, fibroblast growth factor; MIRAS, multiple isomorphous replacement including anomalous scattering; MR, mannose receptor; SBP, sulfate binding protein.

 J. Exp. Med. © The Rockefeller University Press • 0022-1007/2000/04/1105/11 $5.00
Volume 191, Number 7, April 3, 2000 1105–1115
http://www.jem.org/cgi/current/full/191/7/1105

(12, 13). Three-dimensional structures of members of the C-type lectin superfamily (14) have facilitated mechanistic studies of sugar binding by the MR CRDs (15), and the crystal structure of the principal mannose-recognition domain of MR (CRD4) has now been determined.[2]

Recent studies demonstrate that the Cys-MR region also has carbohydrate-binding properties. Cys-MR binds to glycoproteins containing sulfated sugars that terminate in SO_4-4GalNAcβ1,4GlcNAcβ1-, such as the sulfated hormones lutropin and thyroid stimulating hormone (16–18). Further studies of its carbohydrate-recognition properties indicate that Cys-MR can also bind chondroitin sulfates A and B and sulfated oligosaccharides of the Lewis^a and Lewis^x types (19). MR binding of hormones is thought to regulate their bioavailability (20) and facilitate rapid clearance of lutropin from the serum through binding to MR on hepatic endothelial cells (21). Studies using an Fc chimeric protein containing mouse Cys-MR revealed the presence of additional ligand(s) for Cys-MR. The fusion protein binds to cells in germinal centers and to macrophages from the splenic marginal zone and lymph node subcapsular sinus (22). The Cys-MR interaction with cells in the spleen results from the binding of sulfated carbohydrates (19). These results suggest that Cys-MR directs MR-bearing cells toward germinal centers during immune responses, and that sulfated carbohydrate ligands regulate the trafficking and function of cells bearing MR.

To establish the mechanism of sulfated sugar recognition by Cys-MR, we solved crystal structures of Cys-MR alone and complexed with the monosaccharide 4-sulfated-*N*-acetylgalactosamine (4-SO_4-GalNAc). The structures of Cys-MR and the principal mannose-binding domain of MR (CRD4)[2] provide a framework for modeling the structures of domains in the MR family of proteins, and facilitate an understanding of the role of MR in binding carbohydrates in antimicrobial immunity and in hormone regulation.

Materials and Methods

Expression and Purification of Soluble Cys-MR. A Cys-MR-Fc fusion protein (hydrophobic signal sequence and the first 139 residues of mouse MR, a 2-residue linker, and the Fc region of human IgG1) was produced in 293T cells (22). Supernatants from transfected cells were harvested 13 d after transfection. The Cys-MR-Fc protein was collected on protein A beads (Pierce Chemical Co.), eluted with elution buffer (Pierce Chemical Co.), dialyzed into PBS, and concentrated to 5 mg/ml using a centricon filter (Amicon). The chimeric protein was digested with papain coupled to agarose beads (0.4 U/mg of Cys-MR-Fc; Sigma Chemical Co.) in PBS, 10 mM EDTA, 10 mM l-cysteine at 37°C for 1 h. The reaction was terminated by adding iodoacetamide to a concentration of 30 mM and centrifuging out the papain beads. Fc fragments and undigested Cys-MR-Fc were removed using protein A beads. The sequence derived from NH_2-terminal sequencing of purified Cys-MR begins 19 residues after the initiating methionine (NH_2-terminal sequence of mature protein is Leu-Asp-Ala-Arg-Gln; data not shown). Purified human MR starts 18 residues after the initiating methionine with the sequence Leu-Leu-Asp-Ala-Arg-Gln (23), indicating that the position at which the hydrophobic leader peptide is cleaved in the human and mouse versions of MR differs by one residue. The numbering scheme used in this paper corresponds to the numbering of mature mouse Cys-MR.

Crystallization and Data Collection. Crystals (space group $P2_12_12_1$; a = 39.6 Å, b = 41.3 Å, c = 98.8 Å; one molecule per asymmetric unit) were grown at 4°C in 1:1 hanging drops containing Cys-MR (40 mg/ml in 10 mM Hepes, pH 7.4, 10 mM NaCl) and 30% (wt/vol) PEG 8000, 0.2 M $(NH_4)_2SO_4$. Before data collection, crystals were transferred to a cryoprotectant solution (10 mM Hepes, pH 7.0, 32% PEG 8000, 0.2 M $[NH_4]_2SO_4$, 10% glycerol). A native data set used for multiple isomorphous replacement including anomalous scattering (MIRAS) phase determination (Native I; Table I) was collected at –150°C from a single crystal to 1.9 Å using an R-AXIS II detector (Molecular Structures Corp.) mounted on a rotating anode generator (model R200; Rigaku). Heavy atom derivative data sets (prepared by soaking native crystals in synthetic mother liquor containing heavy atoms for 7 d) and the 1.7 Å native data set used for refinement (Native II; Table I) were collected using the same procedures. Crystals in complex with 4-SO_4-GalNAc (space group $P2_12_12_1$; a = 39.4 Å, b = 41.5 Å, c = 100.3 Å; one molecule/asymmetric unit) were obtained by soaking Cys-MR crystals in 2 mM 4-SO_4-GalNAc (Sigma Chemical Co.), 32% PEG 8000, 0.2 M $(NH_4)_2SO_4$ for 10 d at 4°C. Native data were collected to 2.2 Å as described above. Data were processed and scaled with the HKL package (24; Table I).

Structure Determination and Refinement. Heavy atom positions were identified from difference Patterson (mercury derivative) or difference Fourier (platinum derivative) maps. Two mercury and three platinum sites were refined and phases were calculated using SHARP (25). An initial MIRAS electron density map with a mean figure of merit of 0.56 was calculated to 2.5 Å resolution and improved by solvent flattening using Solomon (26). The experimental map was of high quality, with no main chain breaks and clearly identifiable density for most side chains and the unidentified ligand. A skeleton of the map (27) was used as a starting point for model building using the program O (28). Model refinement was performed with CNS (29) using a bulk solvent correction, refinement of individual temperature (B) factors, the maximum likelihood target function, and protocols to minimize R_{free} (30). In later rounds of refinement, water molecules were built into peaks >3.0 σ in difference Fourier maps. The refined model (R_{free} = 20.8%; R_{cryst} = 19.8%) includes residues 2–135 of Cys-MR, 264 water molecules, 1 sulfate group, and no residues in disallowed regions of the Ramachandran plot. There is no ordered density for residues 1 and residues 136–139 of Cys-MR, or for the two-residue linker inserted before the Fc. Ordered density is not observed in the vicinity of the potential N-linked glycosylation site at Asn87.

The structure of Cys-MR complexed with 4-SO_4-GalNAc was solved at 2.2 Å resolution by molecular replacement using native Cys-MR as a search model. The model was refined using CNS (29) as described above. An initial model of 4-SO_4-GalNAc was obtained by combining coordinates for GalNAc and a sulfate group, ensuring proper connectivity and bond angles. The ligand was modeled into a large continuous electron density feature with the sulfate group positioned identically to the sulfate in the native structure. The 4-SO_4-GalNAc molecule is well de-

[2]Feinber, H., S. Park-Snyder, A.R. Kolatkar, C.T. Heise, M.E. Taylor, and W.I. Weis, manuscript submitted for publication.

Table I. *Data Collection, Phasing, and Refinement Statistics*

Data set	Resolution	No. of observations	Unique reflections	Percent complete*	R_{merge}‡	$I/\sigma I$	Phasing power§
	Å				%		
Native I	25.0–1.89	104,666	13,382	98.5	3.8	23.4	
	(1.96–1.89)			(90.2)	(13.3)	(6.6)	
Native II	25.0–1.70	152,280	18,536	98.1	5.5	21.0	
	(1.77–1.70)			(91.3)	(20.5)	(5.9)	
4-SO_4-GalNAc	25.0–2.2	86,630	8,984	97.5	4.5	24.7	
Complex	(2.28–2.20)			(95.5)	(10.5)	(11.8)	
5.0 mM	25.0–2.7	49,974	4,822	93.3	9.0	15.4	2.67
K_2PtCl_4	(2.79–2.70)			(78.4)	(26.8)	(3.7)	
5.0 mM	25.0–2.1	67,012	9,875	98.0	5.3	23.7	1.49
EMP	(2.17–2.10)			(88.7)	(19.0)	(5.7)	

Refinement	Native	4-SO_4-GalNAc complex
Resolution (Å)	25.0–1.7	25.0–2.2
Reflections in working set $\|F\|>0$	17,054	8,156
Reflections in test set $\|F\|>0$	1,078	483
R_{cryst}/R_{free} (%)‖	19.8/20.8	21.3/23.2
Rmsd bond length (Å)	0.008	0.006
Rmsd angles (deg)	1.89	1.49
No. of atoms		
Protein	1,085	1,085
Water	264	153
Ligand	5	19
Ramachandran plot		
Most favored region (%)	86.1	82.8
Additional allowed region (%)	13.9	16.4
Generously allowed region (%)	0.0	0.8
Disallowed region (%)	0.0	0.0

Values in parentheses indicate the high-resolution shells. EMP, ethyl mercury phosphate.
*Complete, no. of independent reflections/total theoretical number.
‡R_{merge} $(I) = [\Sigma|I(i) - <I(h)>|/\Sigma I(i)]$, where $I(i)$ is the ith observation of the intensity of the hkl reflection, and $<I>$ is the mean intensity from multiple measurements of the hkl reflection.
§Phasing power for acentric reflections: rms f_h/E, where f_h is the heavy-atom structure factor amplitude, and E is the residual lack of closure error.
‖R_{cryst} $(F) = \Sigma_h||F_{obs}(h)| - |F_{calc}(h)||/_{-h}|F_{obs}(h)|$, where $|F_{obs}(h)|$ and $|F_{calc}(h)|$ are the observed and calculated structure factor amplitudes for the hkl reflection. R_{free} is calculated over reflections in a test set not included in atomic refinement.

fined in Fo-Fc maps contoured at 3.0 σ and 2Fo-Fc maps contoured at 1.1 σ, with the exception of the *N*-acetyl group, which has weak electron density. The refined model (R_{free} = 23.2%; R_{cryst} = 21.3%) includes 134 amino acids (residues 2–135 of Cys-MR), 153 water molecules, and the 4-SO_4-GalNAc group. None of the residues are in disallowed regions of the Ramachandran plot.

Fig. 1, A and B, Fig. 2, A–D, and Fig. 3, A and B, were made using MOLSCRIPT (31) and Raster3D (32). Electrostatic potentials were calculated, and Fig. 2 E was made using GRASP (33).

Results

Structure Description. Mouse Cys-MR was expressed as an Fc fusion protein and purified from the supernatants of transfected 293T cells. The Cys-MR crystal structure was determined by MIRAS and refined to 1.7 Å resolution (Table I). Cys-MR is a globular protein of approximate dimensions 45 × 40 × 35 Å, which consists of 12 antiparallel β strands arranged in a pattern with approximate threefold internal symmetry (Fig. 1, A and B). Strands 1, 4, 5, 8, 9, and 12 form a centrally-located six-stranded antiparallel β

barrel covered by the remaining β strands. This folding topology, known as a β-trefoil (34), was originally described for the structure of soybean trypsin inhibitor (35), and is found in other proteins such as the ricin B chain (36), fibroblast growth factors (FGFs [37]), IL-1α and β (38, 39), and the actin binding protein hisactophilin (40). Members of this family generally share little or no detectable sequence similarity (Fig. 1 C), but weak sequence similarity between Cys-MR and the ricin B chain was previously reported (41), thus anticipating the structural similarity. Following the conventions for the description of the fold (35, 34), Cys-MR contains three lobes (I, β strands 1–4; II, β strands 5–8; and III, β strands 9–12; Fig. 1, A and B) that are related by approximate three-fold internal symmetry.

The six cysteines for which Cys-MR is named are involved in three disulfide bonds (Fig. 1, A–C). The first, between Cys16 and Cys30, connects β strand 2 and the loop between strands 3 and 4 in lobe I. The second disulfide bond, located in lobe II, is related to the first by the pseudo three-fold symmetry, connecting Cys55 in strand 6 to Cys72 in the loop between strands 7 and 8 (Fig. 1 B). Two disulfide bonds are found in similar positions in the structure of the ricin B chain (Fig. 1, A and C), which allowed correct prediction of the observed disulfide bonding pattern of Cys-MR (41). The third disulfide bond in Cys-MR is not related to the others by the internal three-fold symmetry; instead, it connects Cys83 in strand 8 to the Cys130 in the extended polypeptide chain COOH-terminal to strand 12. This disulfide bond anchors the extended region after strand 12, a feature not found in β-trefoil proteins such as ricin and FGF (Fig. 1 C), to the remainder of the Cys-MR structure. In lobe III, the residues at the positions analogous to the cysteines in lobes I and II are Tyr97 in strand 10 and Gly113 in the loop between strands 11 and 12, whose Cα atoms are separated by 7.1 Å (compared with 5.0 and 5.1 Å for the Cα separation between the cysteines involved in the disulfide bonds in the first two lobes). Even if residues 97 and 113 were substituted by cysteines, a disulfide bond could not form because the Cα atom of residue 113 faces in the opposite direction to the side chain of residue 97 (Fig. 1 B). The reorientation of residue 113 compared with its lobe I and II counterparts occurs because the loop between strands 11 and 12 is shorter than the counterpart loops in lobes I and II (Fig. 1, B and C). Lengthening the loop between strands 11 and 12 would likely disturb ligand binding by Cys-MR, as this

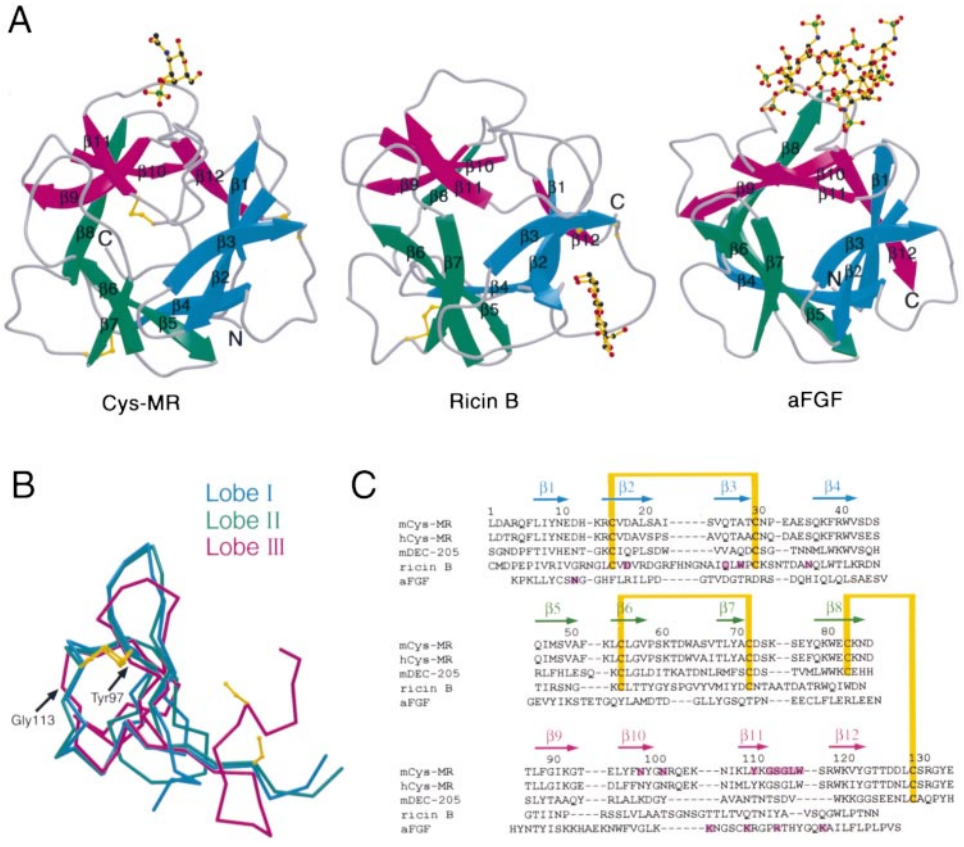

Figure 1. Comparisons between Cys-MR and other β-trefoil proteins. (A) Ribbon diagrams comparing the crystal structures of Cys-MR, a portion of the ricin B chain (residues 1–136 with N-linked carbohydrates omitted; PDB code 2AAI [reference 36]), and human aFGF (PDB code 2AXM [reference 45]). N and C-termini are labeled, disulfide bonds are yellow, and lobes I, II, and III are indicated in different colors. Each structure is depicted with a bound ligand (4-SO_4-GalNAc for Cys-MR, galactose for ricin B chain, and sulfated heparin decasaccharide for aFGF). Rms deviations for Cys-MR superimposed with ricin B chain: 1.6 Å (106 Cαs); Cys-MR superimposed with FGF: 1.9 Å (97 Cαs); ricin B chain superimposed with FGF: 1.6 Å (101 Cαs). (B) Cα superposition of Cys-MR lobes I, II, III based on Cα atoms in β strands. (C) Sequence alignment of Cys-MR and related proteins. Numbering refers to mouse Cys-MR only (see Materials and Methods). The sequences of mouse (m) and human (h) Cys-MR are aligned with mouse DEC-205, human aFGF, and the β-trefoil region of the ricin B chain. Sequences were aligned using ALIGN (available at http://www2.igh.cnrs.fr//bin/align-guess.cgi) in the case of Cys-MR and DEC-205, or based upon structural information for the sequences with known crystal structures, resulting in the following percent amino acid identities: mouse and human Cys-MR: 84%; mouse Cys-MR and DEC-205: 20%; Cys-MR and ricin B chain: 18%; Cys-MR and FGF: 24%; ricin B chain and FGF: 17%. The approximate locations of β strands 1–12 as derived from the structure of mouse Cys-MR are indicated by arrows above the sequences. Yellow lines indicate cysteine residues involved in disulfide bonds in Cys-MR. Ligand-binding residues identified from the crystal structures of Cys-MR bound to 4-SO_4-GalNAc, ricin B bound to galactose (reference 36), and aFGF bound to sulfated heparin decasaccharide are indicated by colored boxes (reference 45).

loop forms the side of the ligand binding pocket (see below).

The Cys-MR structure includes an as yet unidentified ligand that cocrystalizes with the protein. Electron density that cannot be accounted for by the amino acid sequence, N-linked carbohydrate, or water molecules is found in lobe III near the loop connecting strands 11 and 12 (Fig. 2 A, and Table II). Components of the crystallization buffer, which includes ammonium sulfate and Hepes (*N*-[2-hydroxyethyl] piperazine-*N′*-[2-ethanesulfonic acid]; see Materials and Methods), are possible sources of the ligand. A sulfate group fits into the tetrahedral portion of the electron density, and an anomalous difference Fourier map calculated using the native data and refined phases revealed a 7.0 σ peak at the presumed sulfur atom location (Fig. 2 A). The unidentified ligand is unlikely to be ammonium sulfate since the remaining portion of the density is too large to represent an ammonium group and ammonium sulfate is expected to be completely ionized under the near-neutral pH conditions of the crystallization. A molecule of Hepes can be fit into the electron density with its SO_3 group occupying the position of the sulfate group, but there is no density to account for half of the piperazine ring or the hydroxyethyl group. In the absence of conclusive identification of the ligand, it was modeled as a sulfate group in the refined native Cys-MR structure (Table II).

Crystal Structure of Cys-MR Bound to 4-SO_4-GalNAc. To identify the binding site for sulfated carbohydrates on Cys-MR and elucidate the binding interactions, we solved the structure of Cys-MR complexed with 4-SO_4-GalNAc, which was identified as a ligand by its ability to inhibit Cys-MR binding to lutropin (19). The complex structure was determined at 2.2 Å by molecular replacement using data collected from crystals soaked with the ligand. Difference

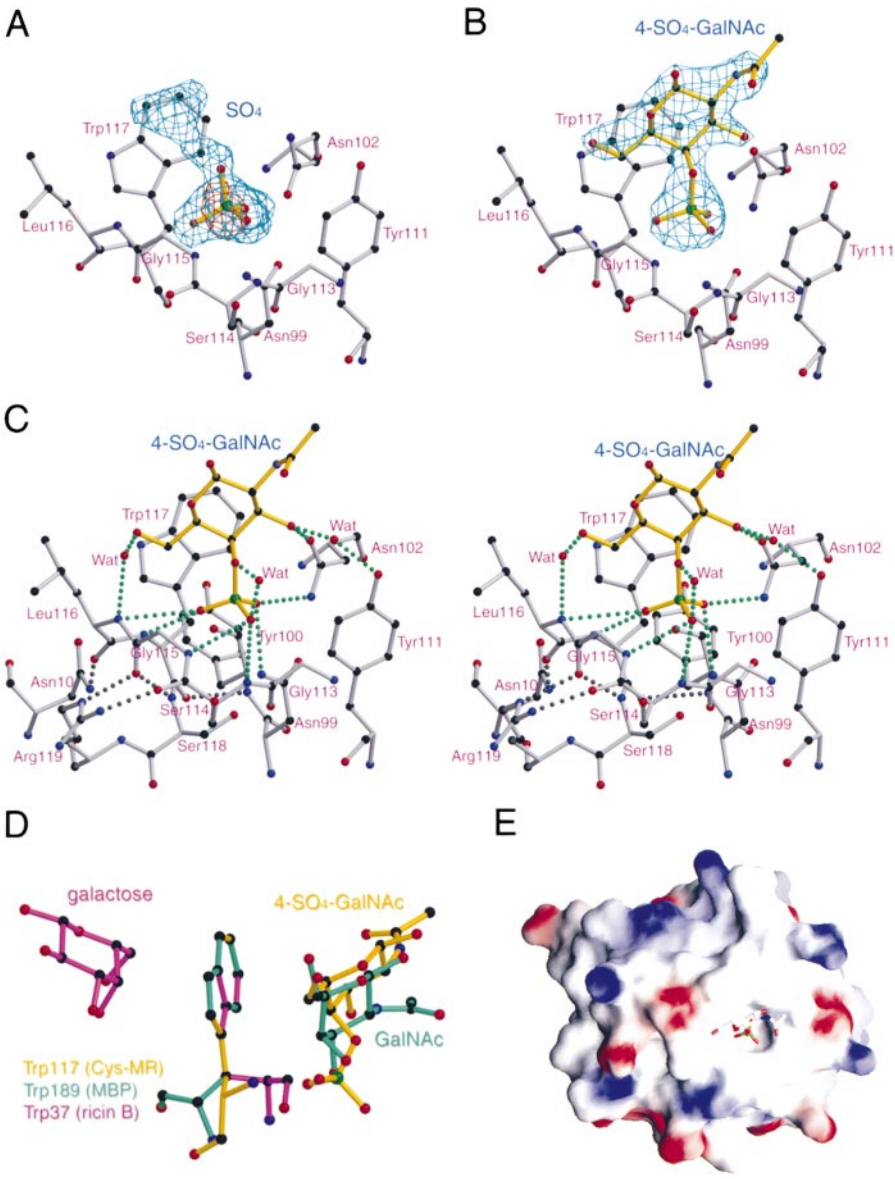

Figure 2. The Cys-MR interaction with ligands. (A) Cys-MR residues in the vicinity of the unidentified ligand (modeled as a sulfate group) derived from the refined model of native Cys-MR. Electron density for the unidentified ligand is indicated in cyan (Fo-Fc map contoured at 3.0 σ) and red (anomalous difference Fourier map contoured at 3.0 σ calculated using native data and refined phases). The peak corresponding to the sulfur of the unidentified ligand (7.5 σ) was the fourth highest peak in the native anomalous difference Fourier. Other peaks are located at the sulfur atoms of the six cysteines and of Met48 (5.5–9.5 σ). (B) Cys-MR residues in the vicinity of 4-SO_4-GalNAc derived from the refined model of the Cys-MR/4-SO_4-GalNAc complex structure. The 4-SO_4-GalNAc ligand is shown superimposed on electron density derived from an Fo-Fc annealed omit map (reference 51) contoured at 3.0 σ. (C) Stereo view of the interaction between 4-SO_4-GalNAc and Cys-MR. Hydrogen bonds between ligand and protein atoms (see Table II) are indicated by dotted green lines. Hydrogen bonds linking the CO groups of residues in which the NH group donates to a sulfate oxygen atom (see text) are indicated by dotted black lines. (D) Comparison of the stacking interactions between tryptophan and galactose rings from the complexed structures of Cys-MR (yellow bonds), the galactose binding mutant of mannose-binding protein (reference 52; PDB code 1AFB, green bonds), and ricin B chain (reference 36; PDB code 2AAI, purple bonds). (E) 4-SO_4-GalNAc is shown on the molecular surface of Cys-MR with colors highlighting the electrostatic potential calculated by GRASP (reference 33). Electrostatic potential is plotted from −10 kT/e (electronegative; red) to +10 kT/e (electropositive; blue), with white indicating electroneutrality.

Table II. *4-SO_4-GalNAc Interactions with Cys-MR*

Between sulfate and Cys-MR					Between GalNAC and Cys-MR			
Bond type	Ligand atom	Protein atom	Distance Complex	Distance Native	Bond type	Ligand atom	Protein atom	Distance
			Å	*Å*				*Å*
H bond	OS1	Asn102 ND2	3.1	3.2	H bond	3-OH	Asn102 OD1	2.6
H bond	OS1	Asn99 ND2	3.2	3.0	H bond	6-OH	Leu116 NH	3.6
H bond	OS2	Ser114 NH	3.5	3.4	H bond	3-OH	Wat-Tyr111 OH	2.9/2.7
H bond	OS2	Gly115 NH	3.2	3.1	H bond	6-OH	Wat-Leu116 NH	3.0/3.2
H bond	OS3	Leu116 NH	3.4	3.3	VDW	C3	Asn102 OD1	3.4
H bond	OS3	Trp117 NH	3.0	2.9	VDW	C3	Trp117 CZ3	3.9
VDW	OS1	Tyr111 CE2	3.5	3.3	VDW	C3	Trp117 CE3	4.0
VDW	OS1	Trp117 CB	3.5	3.7	VDW	C4	Trp117 CD2	3.8
VDW	OS2	Gly115 C	3.2	3.2	VDW	C4	Trp117 CE3	3.4
VDW	OS2	Gly113 CA	3.2	3.4	VDW	C4	Trp117 CZ3	3.8
VDW	OS3	Gly115 C	3.2	3.1	VDW	C5	Trp117 CD2	3.7
VDW	OS3	Gly115 CA	3.1	3.2	VDW	C5	Trp117 CE2	3.9
VDW	OS3	Trp117 CB	3.3	3.3	VDW	C5	Trp117 CE3	3.8
					VDW	C6	Trp117 CG	3.4
					VDW	C6	Trp117 CD1	3.6
			Distance	Distance	VDW	C6	Trp117 CD2	3.4
Bond type	Ligand atom	Ligand atom	Complex	Native	VDW	C6	Trp117 CE2	3.6
H bond	OS2	Wat-OS4	2.8/3.2	2.8/3.4	VDW	C6	Leu116 CD1	3.6
					VDW	6-OH	Leu116 CB	3.4

The following distance and geometry criteria were used for assiging hydrogen bonds: a distance of < 3.5Å, and a hydrogen bond angle of $>90°$. The maximum distance allowed for a van der Waals interaction was 4.0 Å. H bond, hydrogen bond; VDW, van der Waals interaction; Wat, water molecule.

maps reveal unambiguous electron density for the entire ligand, with the sulfate group positioned in the same location as the sulfate of the unidentified ligand found in the native structure (Fig. 2 B, and Table II). The protein portions of both structures are nearly identical (0.34 Å rms deviation for Cα atoms; 0.54 Å rms deviation for all atoms); thus, there are no major main chain or side chain rearrangements induced by ligand binding. Since the Cys-MR binding site is occupied in the native structure, we cannot address whether conformational changes occur upon ligand binding. However, ligand-induced conformational changes have not been observed in other lectin structures, which, in their unoccupied states, generally contain preformed binding sites in which ordered water molecules contribute hydrogen bonds that substitute for hydrogen bonds from the sugar hydroxyls (42).

The 4-SO_4-GalNAc ligand binds in a pocket formed on one side by residues 111–116 in the loop between strands 11 and 12, on the other side by the side chains of residues including Asn102 and Trp117, and on the bottom by the Asn99 side chain. The sulfate portion of 4-SO_4-GalNAc points into the pocket, making extensive hydrogen bonds and van der Waals contacts with residues in the 11–12 loop region (Fig. 2 C). The corresponding region of DEC-205 shares little sequence similarity with Cys-MR and contains a deletion (Fig. 1 C), thus rationalizing the observation that the cysteine-rich domain of DEC-205 does not bind lutropin (19).

The galactose ring of 4-SO_4-GalNAc, which is in the chair conformation, is positioned with the polar A face exposed to solvent and the nonpolar B face stacked against Trp117, making numerous van der Waals interactions with Asn102, Leu116, and Trp117 (Table II, and Fig. 2 D). The stacking interaction between the galactose ring and Trp117 is reminiscent of interactions seen in the structures of other protein–galactose complexes, including plant lectins, bacterial toxins, galectins, and the galactose-binding mutant of mannose-binding protein, in which the nonpolar face of the galactose moiety stacks against the tryptophan or phenylalanine side chains (42; Fig. 2 D). In addition to van der Waals interactions, the 3- and 6-hydroxyl groups of the galactose ring make hydrogen bonds with Asn102 and Leu116, and participate in two water-mediated hydrogen bonds with the protein (Fig. 2 C, and Table II). The *N*-acetyl group makes no contacts with the protein.

The specificity of Cys-MR for sulfated carbohydrates is explained at the structural level by the multitude of interactions between the protein and the sulfate group of 4-SO_4-GalNAc. Of the eight direct hydrogen bonds between Cys-

MR and the ligand, six involve the sulfate group (Table II). The first sulfate oxygen accepts two hydrogen bonds, one from the Asn99 side chain and the other from the Asn102 side chain. The other free oxygens of the sulfate group accept four hydrogen bonds, all involving main chain NH groups of the protein – the NH groups of Ser114 and Gly115 with the sulfate OS2, and the NH groups of Leu116 and Trp117 with the sulfate OS3. The NH groups have no rotational freedom as they are part of the peptide bond, and the residues that they belong to are further constrained by hydrogen bonds involving their peptide CO groups. Thus, the Ser114 CO hydrogen bonds to Arg119 NH_2, the Gly115 CO hydrogen bonds to Ser118 NH and Arg119 NE, the Leu116 CO hydrogen bonds to Asn10 ND2, and the Trp117 CO hydrogen bonds to the NH group of Tyr100. As many of the groups on the protein that are hydrogen bond donors to the sulfate oxygens have no rotational freedom and belong to residues that are constrained in the protein, the precise fold of the polypeptide backbone is critical for the geometry of the Cys-MR ligand binding site.

Although the sulfate portion of 4-SO_4-GalNAc is negatively charged, the binding site on Cys-MR does not have a positive electrostatic potential (Fig. 2 E) and the sulfate group does not interact with positively charged residues or counter ions (Table II). These features are shared with another protein that binds sulfate, the sulfate-binding protein (SBP) from *Salmonella typhimurium* (43). Based on studies of SBP and other proteins that bind charged ligands without using counter ions, a mechanism for stabilizing isolated charges on groups sequestered in proteins was proposed (44). In this mechanism, hydrogen bonds, especially those formed with highly polarized peptide units, stabilize charges on buried groups, which are further dispersed by hydrogen bond arrays. The sulfate binding interactions of both Cys-MR and SBP conform to three common features of proteins that bury isolated negative charges: (1) the interactions are mediated primarily through hydrogen bonds rather than salt bridges or counter ions; (2) most of the hydrogen bonds involve peptide NH groups, and (3) the peptide NH groups associated with the sulfate group are coupled to a hydrogen bond array within the protein.

The Cys-MR ligand binding site differs in many respects from the binding sites of other proteins with β-trefoil folds, including the ricin B chain and FGF, both of which bind carbohydrates. The galactose binding site of the ricin B chain is in lobe I instead of lobe III (Fig. 1, A and C). However, in common with the interaction between the galactose ring of 4-SO_4-GalNAc and Cys-MR, the galactose ligand of ricin B is stacked against a tryptophan residue (Trp37), although, compared with the Cys-MR tryptophan, the opposite face of the ricin tryptophan ring contacts the galactose (Fig. 2 D). While FGF binds a sulfated carbohydrate using a region of its structure analogous to the Cys-MR ligand binding site (the strand 11–12 region of lobe III; Fig. 1, A and C), the FGF site is a fairly flat, positively charged surface that uses electrostatic interactions for ligand recognition (45), by contrast with the neutral pocket that constitutes the Cys-MR binding site, in which electrostatic interactions do not play a role in ligand binding.

Carbohydrate Binding Specificity of Cys-MR. The structure of Cys-MR bound to 4-SO_4-GalNAc can be used to rationalize the observed binding specificity of Cys-MR for sulfated carbohydrates. Biochemical experiments (19) concluded that Cys-MR binds to GalNAc or galactose when it is sulfated on the C3 or C4 position, but only weakly if the sulfate is at the C6 position (19). The lack of discrimination between sulfated galactose and sulfated *N*-acetylgalactosamine is explained by the absence of contacts between the N-acetyl group of 4-SO_4-GalNAc and Cys-MR (Table II). To understand the mechanism that the position of the sulfate is discriminated, we used models of sulfated GalNAc molecules (Fig. 3 A) to predict the interactions between Cys-MR and GalNAc that is sulfated at the C3 or C6 positions and compared these with the interaction observed in the Cys-MR/4-SO_4-GalNAc complex structure. For each carbohydrate model, we positioned the sulfate group in the Cys-MR binding site in the position observed in the crystal structure of Cys-MR complexed with 4-SO_4-GalNAc and allowed rotational freedom about the galactose C6-sulfate oxygen and the galactose C5–C6 bonds. In the case of 3-SO_4-GalNAc, the galactose ring can be fit into the binding site without steric hindrance, making extensive van der Waals contacts with Trp117. The galactose ring of 6-SO_4-GalNAc also fits into the binding site without steric hindrance, but cannot be rotated into a position in which the sugar ring makes extensive van der Waals contacts with Trp117.

The same binding study concluded that Cys-MR recognizes sulfated GalNAc when it is in a terminal, rather than an internal, position within an oligosaccharide chain (19). For example, adding a terminal uronic acid with a β1-3 linkage to a 4-SO_4-GalNAc group prevents binding to Cys-MR. From the mode of binding revealed by the crystal structure, this result is expected since linking a saccharide group to the C3 position of 4-SO_4-GalNAc should prevent access of the sulfate group to the binding site (Fig. 2 C). By contrast, linkage of a sugar to the C1 position of sulfated galactose should not generally affect binding to Cys-MR. Thus, Cys-MR binds chondroitin sulfates that have a terminal 4-sulfated GalNAc with a β1-4 linkage to iduronic acid or to glucuronic acid and also to sulfated blood group carbohydrates with a terminal 3-sulfated galactose joined with a β1-4 or β1-3 linkage to *N*-acetylglucosamine (19). As the hydroxyl group attached to C1 is exposed to solvent in the Cys-MR/4-SO_4-GalNAc structure and is predicted to be exposed on 3-SO_4-GalNAc bound to Cys-MR (Fig. 3 A), it should be possible to link another sugar ring at this position without creating steric hindrance. Thus, it is predicted that the sugar adjoining the terminal sulfated sugar would not contact Cys-MR unless it contained bulky substitutions, thus rationalizing the observation that the identity of the sugar linked to the terminal sulfated carbohydrate did not generally affect the ability to bind to Cys-MR (19).

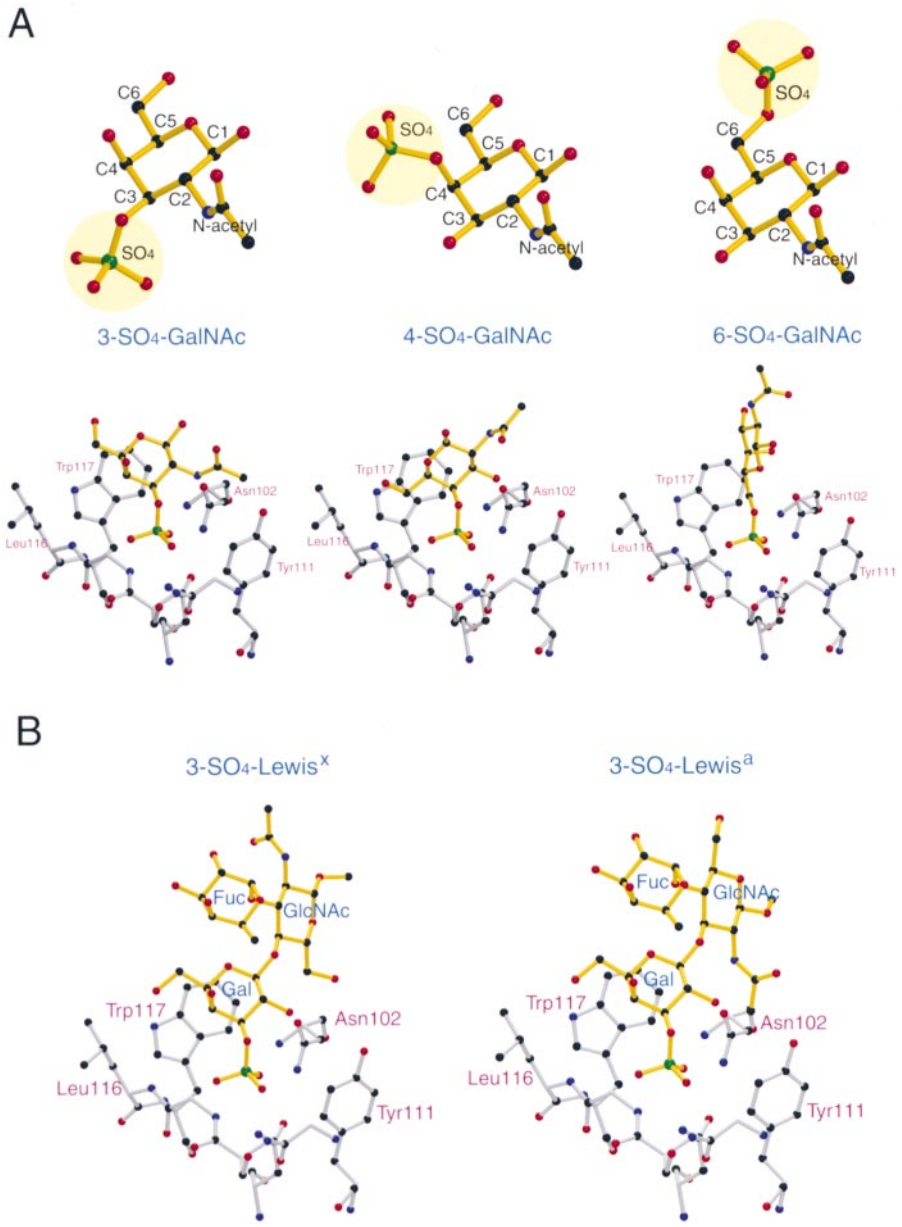

Figure 3. Models of sulfated carbohydrates binding to Cys-MR. (A) Modeled interactions between sulfated GalNAc molecules and Cys-MR. The predicted interactions of Cys-MR with 3-SO_4-GalNAc and 6-SO_4-GalNAc were compared with the observed structure of Cys-MR bound to 4-SO_4-GalNAc. Top: A sulfate group was attached to positions 3 or 6 of the galactose ring of a model of GalNAc (derived from the structure of Cys-MR complexed with 4-SO_4-GalNAc) to produce the sulfated carbohydrate structures shown. Bottom: For each model, the sulfate group was anchored in the Cys-MR binding site as observed in the native and 4-SO_4-GalNAc–complexed Cys-MR structures, and the GalNAc portion was rotated about the galactose C6-sulfate oxygen and C5–C6 bonds to manually arrive at the best fit. (B) Modeled interactions between sulfated Lewis^x and Lewis^a molecules and Cys-MR. The structure of 3-SO_4-Lewis^x was derived from the structures of Lewis^x alone (reference 46) and sulfated Lewis^x bound to a selectin-like mutant of mannose-binding protein (reference 47). The structure of 3-SO_4-Lewis^a was modeled from the 3-SO_4-Lewis^x structure as described (reference 48). 3-SO_4-Lewis^x and 3-SO_4-Lewis^a were modeled into the Cys-MR binding site with their 3-SO_4-galactose rings positioned as in the model of 3-SO_4-GalNAc bound to Cys-MR (A). In this orientation of 3-SO_4-Lewis^a bound to Cys-MR, the *N*-acetyl group on the galactose ring is predicted to clash with Asn102.

Other ligands of Cys-MR include sulfated oligosaccharides of the blood group Lewis^x and Lewis^a series. Lewis^x and Lewis^a saccharides that include a sulfate group at the C3 position of the terminal galactose ring (3-SO_4-Lewis^x and 3-SO_4-Lewis^a) bind Cys-MR, with 3-SO_4-Lewis^x binding slightly (approximately three-fold) better than 3-SO_4-Lewis^a (19). To model the interaction between Cys-MR and sulfated Lewis^x, we used a model of 3-SO_4-Lewis^x derived from the structures of Lewis^x alone (46) and sulfated Lewis^x bound to a selectin-like mutant of mannose-binding protein (47). The structure of 3-SO_4-Lewis^a was modeled from the 3-SO_4-Lewis^x structure as described (48). The 3-SO_4-galactose portions of 3-SO_4-Lewis^x and 3-SO_4-Lewis^a (Fig. 3 B) were superimposed with the model of 3-SO_4-GalNAc bound to Cys-MR (Fig. 3 A), allowing rotational freedom about the sulfo–galactose bond. In the case of 3-SO_4-Lewis^x, a stacking interaction between Trp117, the sulfated galactose ring, and the fucose ring is predicted (Fig. 3 B). When 3-SO_4-Lewis^a is positioned similarly in the binding site, the *N*-acetyl portion of the glucose ring of Lewis^a clashes with Cys-MR residue Asn102 (Fig. 3 B), which may account for the observed preference for 3-SO_4-Lewis^x over 3-SO_4-Lewis^a (19).

Discussion

MR is a carbohydrate-binding receptor that contains regions with distinct carbohydrate-recognition properties.

The first involves binding of C-type lectin CRDs to glycans that terminate with mannose, fucose, or *N*-acetylglucosamine residues. The second involves binding of the NH_2-terminal Cys-MR domain to acidic glycans such as those terminating with 4-sulfated *N*-acetylgalactosamine or 3-sulfated galactose. Ligands for the CRDs include carbohydrates on the surfaces of infectious agents; thus, MR is thought to serve as a pattern-recognition receptor in the innate immune response and to deliver carbohydrate-containing antigens to MHC molecules for antigen presentation in the adaptive immune response (4). In addition, the MR CRDs have recently been shown to bind to pituitary hormones, most likely through interactions involving terminal mannose or core fucose residues (49). Carbohydrate-containing ligands for the Cys-MR domain include endogenous proteins such as sulfated pituitary hormones (16–18) and molecules expressed on cells in the spleen and germinal centers (19, 22). The dual carbohydrate specificity of MR gives it the potential to serve as a bridge between ligands containing nonacidic glycans such as mannose and those containing acidic sulfated glycans. For example, macrophages secrete a soluble form of MR (50), which has been proposed to direct mannose-bearing antigens to cells expressing Cys-MR ligand(s) at sites where humoral immune responses take place (22, 50).

The two types of carbohydrate-binding regions of MR have different structures and sugar-binding properties. The eight CRDs of MR are predicted to fold into structures resembling C-type lectin domains (4, 14), as recently confirmed by the crystal structure of MR CRD4.[2] The CRD fold contains α-helical and β-strand secondary structural elements and regions with no ordered secondary structure that include the calcium-binding loops (14, 42). Calcium is required for the integrity of the fold and for binding carbohydrates, such that a calcium ion forms direct coordination bonds with mannose, fucose, *N*-acetylglucosamine, and glucose molecules. Protein–ligand interactions in CRDs include hydrogen bonds between the sugar hydroxyls and protein side chains (14, 42). The fold of the NH_2-terminal Cys-MR region, the other carbohydrate-binding portion of MR, bears no resemblance to CRDs. Instead, Cys-MR is a member of the β-trefoil family of proteins, which are approximately three-fold symmetric structures composed of 12 β strands (34). Other β-trefoil proteins, such as acidic FGF (aFGF) and the trefoil region of the ricin B chain, bind carbohydrates, but their binding sites and mechanisms of carbohydrate recognition differ from those of Cys-MR (Fig. 1 A). Thus, the Cys-MR binding site and residues critical for ligand recognition could not have been predicted from structural comparisons, but were revealed in the crystal structure of Cys-MR complexed with 4-SO_4-GalNAc. The binding site is a neutral pocket that accommodates the sulfate group, with numerous hydrogen bonds between the sulfate oxygens and protein atoms, primarily main chain NH groups, which serve to disperse the negative charge. Although the galactose ring of the ligand makes specific contacts with Cys-MR, the majority of interactions involve the sulfate group, rationalizing the specificity of Cys-MR for acidic carbohydrate ligands such as sulfated galactose (4).

Identification of the residues in the Cys-MR binding site facilitates comparisons with the sequences of cysteine-rich regions of other proteins in the MR family. The cysteine-rich domains of other members of the MR family, including DEC-205 (10) and the phospholipase A2 receptor (7–9), contain a deletion in their sequences in the region analogous to that used by Cys-MR for binding 4-SO_4-GalNAc (Fig. 1 C). Thus, these receptors are not predicted to bind sulfated carbohydrates using in a manner analogous to Cys-MR, consistent with the observation that this region of DEC-205 does not bind lutropin (19). Together with the structure of CRD4,[2] the structure of Cys-MR provides a structural framework to evaluate sugar recognition by the two types of carbohydrate-binding portions of the MR family of proteins.

We thank S. Gordon and L. Martínez-Pomares for the Cys-MR-Fc expression vector, G. Hathaway and the California Institute of Technology's Protein/Peptide Micro Analytical Laboratory for peptide analyses, M.J. Bennett, A.P. Yeh, L.M. Sanchez, H.J. Chiu, S. Ding, and M. Williamson for crystallographic assistance, and W.I. Weis, M.E. Taylor, and members of the Bjorkman laboratory for critical reading of the manuscript. Coordinates have been submitted to the Protein Data Bank (available at www.rcsb.org/pdb/ under accession nos. IDQG and IDQO).

This work was supported by the Howard Hughes Medical Institute (P.J. Bjorkman and M.C. Nussenzweig) and grants from the National Institutes of Health (M.C. Nussenzweig). Y. Liu was a recipient of Ferguson Fund predoctoral Fellowship and Teaching Assistantship (California Institute of Technology).

Submitted: 7 December 1999
Revised: 27 January 2000
Accepted: 4 February 2000

References

1. Janeway, C.A., Jr. 1992. The immune system evolved to distinguish infectious nonself from non-infectious self. *Immunol. Today*. 13:11–16.
2. Takahashi, K., M.J. Donovan, R.A. Rogers, and R.A.B. Ezekowitz. 1998. Distribution of murine mannose receptor expression from early embryogenesis through to adulthood. *Cell Tissue Res*. 292:311–323.
3. Linehan, S.A., L. Martínez-Pomares, P.D. Stahl, and S. Gordon. 1999. Mannose receptor and its putative ligands in normal murine lymphoid and nonlymphoid organs: in situ expression of mannose receptor by selected macrophages, endothelial cell, perivascular microglia, and mesangial cells, but not dendritic cells. *J. Exp. Med*. 189:1961–1972.
4. Stahl, P.D., and R.A.B. Ezekowitz. 1998. The mannose receptor is a pattern recognition receptor involved in host defense. *Curr. Opin. Immunol*. 10:50–55.
5. Sallusto, F., M.I. Cella, C. Danieli, and A. Lanzavecchia. 1995. Dendritic cells use macropinocytosis and the mannose receptor to concentrate macromolecules in the major histocompatibility complex class II compartment: downregulation by cytokines and bacterial products. *J. Exp. Med*. 182:389–400.
6. Prigozy, T.I., P.A. Sieling, D. Clemens, P.L. Stewart, S.M.

Behar, S.A. Porcelli, M.B. Brenner, R.L. Modlin, and M. Kronenberg. 1997. The mannose receptor delivers lipoglycan antigens to endosomes for presentation to T cells by CD1b molecules. *Immunity*. 6:187–197.

7. Ishizaki, J., K. Hanasaki, K. Higashino, J. Kishimo, N. Kikuchi, O. Ohara, and H. Arita. 1994. Molecular cloning of pancreatic group I phospholipase A2 receptor. *J. Biol. Chem.* 269:12156–12162.
8. Lambeau, G., P. Ancian, J. Barhanin, and M. Lazdunski. 1994. Cloning and expression of a membrane receptor for secretory phospholipases A_2. *J. Biol. Chem*. 269:1575–1578.
9. Ancian, P., G. Lambeau, M.-G. Madei, and M. Lazdunski. 1995. The human 180 kDa receptor for secretory phospholipases A_2. *J. Biol. Chem.* 270:8963–8970.
10. Jiang, W.P., W.J. Swiggard, C. Heufler, M. Peng, A. Mirza, R.M. Steinman, and M.C. Nussenzweig. 1995. The receptor DEC-205 expressed by dendritic cells and thymic epithelial cells is involved in antigen processing. *Nature*. 375:151–155.
11. Wu, K., J. Yuan, and L.A. Lasky. 1996. Characterization of a novel member of the macrophage mannose receptor type C lectin family. *J. Biol. Chem.* 271:21323–21330.
12. Taylor, M.E., K. Bezouska, and K. Drickamer. 1992. Contribution to ligand binding by multiple carbohydrate recognition domains in the macrophage mannose receptor. *J. Biol. Chem.* 267:1719–1726.
13. Taylor, M.E., and K. Drickamer. 1993. Structural requirements for high affinity binding of complex ligands by the mannose receptor. *J. Biol. Chem*. 268:399–404.
14. Weis, W.I., M.E. Taylor, and K. Drickamer. 1998. The C-type lectin superfamily in the immune system. *Immunol. Rev*. 163:19–34.
15. Mullin, N.P., P.G. Hitchen, and M.E. Taylor. 1997. Mechanism of Ca_2^+ and monosaccharide binding to a C-type carbohydrate-recognition domain of the macrophage mannose receptor. *J. Biol. Chem*. 272:5668–5681.
16. Fiete, D., and J.U. Baenziger. 1997. Isolation of the SO_4-4-GalNAcβ1, 4GlcNAcβ1, 2Manα-specific receptor from rat liver. *J. Biol. Chem.* 272:14629–14637.
17. Fiete, D., M.C. Beranek, and J.U. Baenziger. 1997. The macrophage endothelial cell mannose receptor cDNA encodes a protein that binds oligosaccharides terminating with SO_4-4-GalNAcβ1,4GlcNAcβ or Man at independent sites. *Proc. Natl. Acad. Sci. USA*. 94:11256–11261.
18. Fiete, D.J., M.C. Beranek, and J.U. Baenziger. 1998. A cysteine-rich domain of the "mannose" receptor mediates GalNAc-4-SO_4 binding. *Proc. Natl. Acad. Sci. USA*. 95:2089–2093.
19. Leteux, C., W. Chai, R.W. Loveless, C.-T. Yuen, L. Uhlin-Hansen, Y. Combarnous, M. Jankovic, S.C. Maric, Z. Misulovin, M.C. Nussenzweig, and T. Feizi. 2000. The cysteine-rich domain of the macrophage mannose receptor is a multispecific lectin which recognizes chondroitin sulfates A and B and sulfated oligosaccharides of blood-group Lewis^a and Lewis^x types in addition to the sulfated *N*-glycans of luteinizing hormone. *J. Exp. Med.* 191:1117–1126.
20. Baenziger, J.U., S. Kumar, R.M. Brodbeck, P.L. Smith, and M.C. Beranek. 1992. Circulatory half-life but not interaction with the lutropin chorionic-gonadotropin receptor is modulated by sulfation of bovine lutropin oligosaccharides. *Proc. Natl. Acad. Sci. USA*. 89:334–338.
21. Smith, P.L., G.R. Bousfield, S. Kuman, D. Fiete, and J.U. Baenziger. 1993. Equine lutropin and chorionic gonadotropin bear oligosaccharides terminating with SO_4-4-GalNAc and Sia-α-2,3Gal, respectively. *J. Biol. Chem.* 268:795–802.
22. Martínez-Pomares, L., M. Kosco-Vilbois, E. Darley, P. Tree, S. Herren, J.-Y. Bonnefoy, and S. Gordon. 1996. Fc chimeric protein containing the cysteine-rich domain of the murine mannose receptor binds to macrophages from splenic marginal zone and lymph node subcapsular sinus and to germinal centers. *J. Exp. Med.* 184:1927–1937.
23. Taylor, M.E., J.T. Conary, M.R. Lennartz, P.D. Stahl, and K. Drickmer. 1990. Primary structure of the mannose receptor contains multiple motifs resembling carbohydrate-recognition domains. *J. Biol. Chem.* 265:12156–12162.
24. Otwinowski, Z., and W. Minor. 1997. Processing of X-ray diffraction data collected in oscillation mode. *Methods Enzymol.* 276:307–326.
25. De La Fortelle, E., and G. Bricogne. 1997. Maximum-likelihood heavy-atom parameter refinement for multiple isomorphous replacement and multiwavelength anomalous diffraction methods. *Methods Enzymol.* 276:472–494.
26. Abrahams, J.P., and A.G.W. Leslie. 1996. Methods used in the structure determination of bovine mitochondrial F1 ATPase. *Acta Crystallogr. D*. 52:30–42.
27. Kleywegt, G.J., and T.A. Jones. 1997. Template convolution to enhance or detect structural features in macromolecular electron density maps. *Acta Crystallogr. D*. 53:179–185.
28. Jones, T.A., and M. Kjeldgaard. 1997. Electron density map interpretation. *Methods Enzymol*. 277:173–208.
29. Brünger, A.T., P.D. Adams, G.M. Clore, P. Gros, R.W. Grosse-Kunstleve, J.-S. Jiang, J. Kuszewski, M. Nilges, N.S. Pannu, R.J. Read, et al. 1998. Crystallography and NMR system: a new software system for macromolecular structure determination. *Acta Crystallogr. D*. 54:905–921.
30. Brünger, A.T. 1992. Free R value: a novel statistical quantity for assessing the accuracy of crystal structures. *Nature*. 355: 472–475.
31. Kraulis, P.J. 1991. MOLSCRIPT: a program to produce both detailed and schematic plots of protein structures. *J. Appl. Crystallogr*. 24:946–950.
32. Merritt, E.A., and M.E.P. Murphy. 1994. Raster3D version 2.0, a program for photorealistic molecular graphics. *Acta Crystallogr. D*. 50:869-873.
33. Nicholls, A., R. Bharadwaj, and B. Honig. 1993. GRASP: graphical representation and analysis of surface properties. *Biophys. J.* 64:A166.
34. Murzin, A.G., A.M. Lesk, and C. Chothia. 1992. Beta-trefoil fold patterns of structure and sequence in the Kunitz inhibitors, interleukins-1β and 1α and fibroblast growth factors. *J. Mol. Biol.* 223:531–543.
35. McLachlan, A.D. 1979. Three-fold structural pattern in the soybean trypsin inhibitory (Kunitz). *J. Mol. Biol.* 133:557–563.
36. Rutenber, E., and J.D. Robertus. 1991. Structure of ricin B-chain at 2.5 Å resolution. *Proteins*. 10:260–269.
37. Zhu, X., H. Komiya, A. Chirino, S. Faham, G.M. Fox, T. Arakawa, B.T. Hsu, and D.C. Rees. 1991. Three-dimensional structures of acidic and basic fibroblast growth factors. *Science*. 251:90–93.
38. Finzel, B.C., L.L. Clancy, D.R. Holland, S.W. Muchmore, K.D. Watenpaugh, and H.M. Einspahr. 1989. Crystal structure of recombinant human interleukin-1β at 2.0 Å resolution. *J. Mol. Biol*. 209:779–791.
39. Graves, B.J., M.H. Hatada, W.A. Hendrickson, J.K. Miller, V.S. Madison, and Y. Satow. 1990. Structure of interleukin-1α at 2.7 Å resolution. *Biochemistry*. 29:2679–2684.

40. Habazetti, J., D. Gondol, R. Wiltscheck, J. Otlewski, M. Schleicher, and T.A. Holak. 1992. Structure of hisactophilin is similar to interleukin-1β and fibroblast growth factor. *Nature*. 359:855–858.
41. Harris, N., L.L. Peters, E.M. Eicher, M. Rits, D. Raspberry, Q.G. Eichbaum, M. Super, and R.A. Ezekowitz. 1994. The exon-intron structure and chromosomal localization of the mouse macrophage mannose receptor gene Mrc1: identification of a ricin-like domain at the N-terminus of the receptor. *Biochem. Biophys. Res. Commun.* 198:682–692.
42. Weis, W.I., and K. Drickamer. 1996. Structural basis of lectin-carbohydrate recognition. *Annu. Rev. Biochem.* 65:441–473.
43. Pflugrath, J.W., and F.A. Quiocho. 1988. The 2 Å resolution structure of the sulfate-binding protein involved in active transport in *Salmonella typhimurium*. *J. Mol. Biol.* 200:163–180.
44. Quiocho, F.A., J.S. Sack, and N.K. Vyas. 1987. Stabilization of charges on isolated ionic groups sequestered in proteins by polarized peptide units. *Nature*. 329:561–564.
45. DiGabriele, A.D., I. Lax, D.I. Chen, C.M. Svahn, M. Jaye, J. Schlessinger, and W.A. Hendrickson. 1998. Structure of a heparin-linked biologically active dimer of fibroblast growth factor. *Nature*. 393:812–817.
46. Perez, S., N. Mouhous-Riou, N.E. Nifant'ev, Y.E. Tsvetkov, B. Bachet, and A. Imberty. 1996. Crystal and molecular structure of a histo-blood group antigen involved in cell adhesion: the Lewis^x trisaccharide. *Glycobiology*. 6:537–542.
47. Ng, K.K.-S., and W.I. Weis. 1997. Structure of a selectin-like mutant of mannose binding protein complexed with sialylated and sulfated Lewis^x oligosaccharides. *Biochemistry*. 36: 979–988.
48. Kogelberg, H., T.A. Frenkiel, S.W. Homans, A. Lubineau, and T. Feizi. 1996. Conformational studies on the selectin and natural killer cell receptor ligands sulfo- and sialyl-lacto-*N*-fucopentaoses (SuLNFPII and SLNFPII) using NMR spectroscopy and molecular dynamics simulations. Comparisons with the nonacidic parent molecule LNFPII. *Biochemistry*. 35:1954–1964.
49. Simpson, D.Z., P.G. Hitchen, E.L. Elmhirst, and M.E. Taylor. 1999. Multiple interactions between pituitary hormones and the mannose receptor. *Biochem. J.* 343:403–411.
50. Martínez-Pomares, L., J.A. Mahoney, R. Káposzta, S.A. Linehan, P.D. Stahl, and S. Gordon. 1998. A functional soluble form of the murine mannose receptor is produced by macrophages in vitro and is present in mouse serum. *J. Biol. Chem.* 273:23376–23380.
51. Hodel, A., S.-H. Kim, and A.T. Brünger. 1992. Model bias in macromolecular crystal structures. *Acta Crystallogr. A*. 48: 851–858.
52. Kolatkar, A.R., and W.I. Weis. 1996. Structural basis of galactose recognition by C-type animal lectins. *J. Biol. Chem.* 271:6679–6685.